




Review

Differential Antennas: Fundamentals and Applications

Yueping Zhang 

Nanyang Technological University, 639698, Singapore

Corresponding author: Yueping Zhang, Email: eypzhang@ntu.edu.sg.

Received September 22, 2022; Accepted December 12, 2022; Published Online March 31, 2023.

Copyright © 2023 The Author(s). This is a gold open access article under a Creative Commons Attribution License (CC BY 4.0).

Abstract — Driven by the great demand for highly integrated wireless system-on-chip and system-in-package devices, there has recently been increasing interest in the research and development of differential antennas. Many studies on the design, analysis, and measurement of differential antennas have been published. This paper presents an overview of the fundamentals and applications of differential antennas. First, it compares differential to balanced and single-ended to unbalanced antennas and explains why the new terms (differential and single-ended antennas) should be adopted instead of the old terms (balanced and unbalanced antennas). Second, it addresses the quantitative relationship between a differential antenna and its single-ended counterpart, which is important and useful because the properties of either the differential or single-ended antenna can be determined from the other with a known solution. Third, it describes how differential antennas can be measured, with a special emphasis on the balun method. Fourth, it classifies differential antennas into wire, slot, microstrip, printed, and dielectric resonator antennas to better present their suitability and functionality. Fifth, it provides application examples of differential antennas from simple discrete wire to sophisticated microstrip designs. Finally, it is argued that the old paradigms of lower gains and bulkier sizes of differential antennas as compared to single-ended antennas do not always hold true; for instance, differential microstrip patch antennas can possess comparable or even smaller sizes and higher gain values than single-ended microstrip patch antennas.

Keywords — Differential antennas, Single-ended antennas, Balanced antennas, Unbalanced antennas, Antenna-in-package, Antenna-on-chip.

Citation — Yueping Zhang, “Differential Antennas: Fundamentals and Applications,” *Electromagnetic Science*, vol. 1, no. 1, article no. 0010021, 2023. doi: [10.23919/emsci.2022.0002](https://doi.org/10.23919/emsci.2022.0002).

I. Introduction

Antennas were first created as dipoles and loops by Heinrich Hertz, who used them from 1886 to 1888 to demonstrate the existence of electromagnetic waves and to validate Maxwell’s theory [1]. Antennas were then made as monopoles by Guglielmo Marconi, who began to use them in radio transmission experiments in 1895 [2]. Since then, many forms of antennas, such as reflector, horn, lens, Yagi-Uda, slot, helix, spiral, log-periodic, microstrip patch antennas, and dielectric resonator antennas, have been developed for various applications [3]–[10].

It has been customary to refer to antennas as either balanced or unbalanced antennas [11]. However, the dichotomy of antennas as being balanced or unbalanced according to their structures can cause confusion in practice. For example, the existence of any metallic object in the vicinity of a balanced antenna will likely modify it to being an unbalanced antenna. An off-centered excitation of a balanced antenna as used for impedance matching will also turn the device into an unbalanced antenna. The ground plane of a modern radio-frequency (RF) system-on-chip (SoC) or system-in-package (SiP) module may be much smaller than one free-space wavelength. The system ground plane shared by an unbalanced antenna also contributes to radiation. In

this case, the unbalanced antenna has been somewhat changed into a balanced antenna.

Now, it is thus opportune to distinguish antennas by their sources as differential and single-ended, because the trend of codesign and joint integration of antennas and circuits for modern RF SoC or SiP modules has generated the need to optimize the antennas and circuits as a whole. Optimization is typically done in a circuit simulator using extracted compact models of antennas given by an electromagnetic solver [12]. In the circuit community, the terms of differential and single-ended circuits prevail over those of balanced and unbalanced circuits [13]. Therefore, it is better for integrated antenna designers to adopt the terms of differential and single-ended antennas to avoid any potential misunderstanding from integrated circuit designers [14]–[39].

Differential circuits permit higher linearity and lower offset, leaving them more immune to power supply variations, temperature changes, and substrate noise than single-ended circuits. Consequently, differential circuits are more popular than single-ended circuits in integrated circuit design.

Single-ended antennas such as monopoles show higher gain values and smaller radiator sizes than differential antennas such as dipoles. Therefore, single-ended antennas

have dominated the design of discrete antennas for conventional RF systems. However, it must be stressed that the concept of lower gains and bulkier sizes of differential antennas compared to single-ended antennas is not always true. It has been demonstrated that differential microstrip patch antennas can possess comparable or even smaller sizes and higher gain values than single-ended microstrip patch antennas [22]–[24].

Differential circuits naturally call for differential antennas, which is particularly essential in the design of an RF SoC or SiP. Taking the RF SoC in a 65-nm complementary metal oxide semiconductor (CMOS) process as an example, the voltage supply for the integrated circuits fabricated in CMOS technology is typically 1.2 V. With this low voltage level, a differential power amplifier can theoretically yield 3 dB greater RF power than a single-ended power amplifier. Furthermore, differential antennas perfectly interconnect with differential circuits. No lossy balanced/unbalanced conversion circuit (balun) is needed. As a result, the receiver noise performance and transmitter power efficiency are improved [25]–[27].

This paper aims to provide an overview of differential antennas [28]–[89]. To the best of the author's knowledge, this is the first review paper on differential antennas. Section II describes the theory of differential antennas and the relationship between a differential antenna and its single-ended counterpart. Section III presents differential antenna measurements with special emphasis given to the balun method. Section IV classifies differential antennas and examines their suitability. Section V highlights some important applications of differential antennas. Section VI summarizes conclusions and identifies future directions.

II. Theory of Differential Antennas

A differential antenna is an antenna with two input terminals receiving a differential signal source V_d . A single-ended antenna is an antenna with a single input terminal receiving a single-ended signal source V_s [37]. Figure 1 shows such a differential antenna and its single-ended counterpart. Note that the differential antenna contains two input terminals but no ground plane, and the single-ended antenna contains one input terminal and the ground plane.

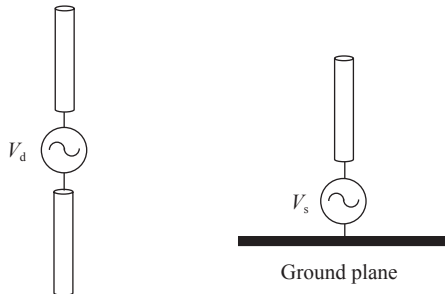


Figure 1 Illustration of a differential antenna and its single-ended counterpart where $V_d = 2V_s$.

A differential antenna can also be an antenna having two single-ended input ports. Each single-ended input port

must receive a single-ended signal source V_s . The two single-ended signal sources applied on the two single-ended input ports should present the same amplitude but opposite phases. The single-ended counterpart of such a differential antenna possesses one single-ended input port excited by a single-ended signal source V_s , while the other single-ended input port maintains an open-circuit configuration [37]. Figure 2 shows such a differential antenna and its single-ended counterpart. Note that both antennas contain ground planes.

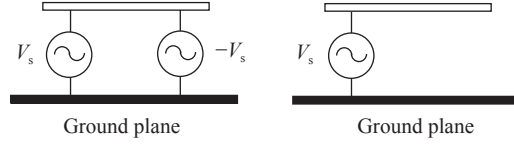


Figure 2 Illustration of another differential antenna and its single-ended counterpart.

1. Input impedances

The circuit parameter of impedance is used to characterize the input to an antenna with respect to a signal source. Let us consider a two-port antenna. The differential input impedance of the two-port antenna can be expressed as

$$Z_{\text{dif}} = Z_{11} - Z_{12} - Z_{21} + Z_{22} \quad (1)$$

where Z_{11} and Z_{22} are the self-impedances at the two single-ended input ports and Z_{12} and Z_{21} are the mutual impedances between the two single-ended input ports. The single-ended input impedances of the two-port antenna can be expressed as

$$Z_{\text{sig1}} = Z_{11} \quad (2)$$

$$Z_{\text{sig2}} = Z_{22} \quad (3)$$

Normally, a two-port antenna designed as a differential antenna is symmetric; therefore, (1), (2), and (3) reduce to

$$Z_{\text{dif}} = 2(Z_{11} - Z_{12}) = 2(Z_{22} - Z_{21}) \quad (4)$$

$$Z_{\text{sig1}} = Z_{\text{sig2}} = Z_{\text{sig}} = Z_{11} \quad (5)$$

It is known that there exist relations to translate from differential antennas to their single-ended counterparts and vice versa [37]. Quantitative relations are given by

$$\frac{Z_{\text{dif}}}{Z_{\text{sig}}} = \begin{cases} 2, & \text{for } Z_{12} = 0 \\ 4, & \text{for } Z_{12} = -Z_{11} \\ 0, & \text{for } Z_{12} = Z_{11} \end{cases} \quad (6)$$

which indicates that an unknown antenna impedance can be determined from the corresponding known impedance [37]. A ratio of 2 is determined from image theory for the antennas in Figure 1. A ratio of 4 can be proven for the same complex power to the antennas in Figure 2 based on

$$\frac{Z_{\text{dif}}}{Z_{\text{sig}}} = \frac{|I_{\text{sig}}|^2}{|I_{\text{dif}}|^2} = \frac{|I_{\text{sig}}|^2}{\left|\frac{1}{2}I_{\text{sig}}\right|^2} = 4 \quad (7)$$

where I_{sig} and I_{dif} represent the currents from the single-ended and configured differential signal sources to the antennas, respectively. The ratio equaling 4 is significant for impedance matching. For instance, if both single-ended antennas and circuits are designed for input impedances of 50Ω , they are matched to each other and can be directly connected. However, if they are mirrored to become differential antennas and circuits, the input impedance of the differential antenna is 200Ω , while the input impedance of the differential circuit is 100Ω . Thus, they are mismatched to each other. In this context, the single-ended input impedance of a differential antenna should be designed to be 25Ω for natural integration with the differential circuit of 100Ω . A ratio of 0 can exist if the two-port antenna operates in a higher-order mode for the differential operation and in a fundamental mode for the single-ended operation at the same frequency [37].

2. Radiation characteristics

The radiation characteristics of an antenna are quantified in the far-field region by the directivity, efficiency, polarization, pattern, etc.

For the differential antenna and its single-ended counterpart in Figure 1, according to image theory, the radiation characteristics can be determined from the other antenna with known radiation characteristics [11]. For example, the half-wavelength dipole and quarter-wavelength monopole are the differential and single-ended counterpart antennas. These systems should possess the same efficiency and polarization. The directivity of the differential dipole should be half that of the single-ended monopole, or the directivity of the single-ended monopole should be twice that of the half-wavelength dipole.

For the differential antenna and its single-ended counterpart in Figure 2, it has been found that the differential antenna provides a desirable cancellation mechanism, which leads to a more symmetrical radiation pattern and a lower cross-polarization radiation level than the single-ended counterpart.

III. Measurement of Differential Antennas

Differential antenna measurements are performed to determine the differential input impedance and radiation characteristics. Experience informs that it is inconvenient to perform differential antenna measurements because most antenna laboratories are equipped with conventional two-port vector network analysers, which are designed for single-ended antenna measurements. Nevertheless, three methods to measure the input impedance of a differential antenna have been reported and compared [40], and one method has been developed to measure the radiation characteristics of the differential antenna [17].

The three methods for the measurement of the input impedance of the differential antenna are: the standard S -parameter, mixed-mode S -parameter, and balun methods. The standard S -parameter method was reported by Meys

and Janssens [41] and later improved by Palmer and Rooyen [42]. It is likely the easiest method, but does not provide any differential excitation to the antennas. First, the two-port vector network analyzer (VNA) is calibrated. Second, the two-port S -parameters are measured with the differential antenna under test (DUT) in place. Finally, the input impedance of the DUT is derived from the S parameters as

$$Z_{\text{dif}} = 2Z_0 \frac{1 - S_{11}S_{22} + S_{12}S_{21} - S_{12} - S_{21}}{(1 - S_{11})(1 - S_{22}) - S_{21}S_{12}} \quad (8)$$

where Z_0 is the reference impedance of 50Ω .

The mixed-mode S -parameter method is certainly the most sophisticated method, but it requires a more expensive and less accessible four-port VNA. First, the four-port VNA is calibrated. Second, the unused two ports are terminated with matched loads or left open. Third, the mixed-mode S parameters are measured with the DUT in place and under true differential stimulus signals of identical amplitude and with a 180° phase shift directly at the DUT. Finally, the input impedance of the DUT is derived from the mixed-mode S parameters as

$$Z_{\text{dif}} = 2Z_0 \frac{1 + S_{\text{d}11}}{1 - S_{\text{d}11}} \quad (9)$$

The balun method uses a two-port VNA and a balun. The balun is typically either a three-port 180° power divider or a four-port 180° hybrid junction. The balun method avoids the problems of the standard and mixed-mode S -parameter methods, but removing the effect of the balun is quite complicated. Hence, most reported impedance results of differential antennas are actually the characteristics of balun-antenna combinations [15], [16]. Zhang and Tu proposed a calibration technique to remove the effects of the three-port 180° power divider [43].

Figure 3 shows the measurement setup for the balun method. The DUT is fed by a two-port VNA although a three-port 180° power divider as the balun. First, a full two-port calibration of the VNA to the coaxial cables (used to connect to the balun) is performed. The VNA can then be considered ideal at the end of the coaxial cables. Second, the two-port S -parameters of the ten two-port standards with the VNA are measured. The ten two-port standards are

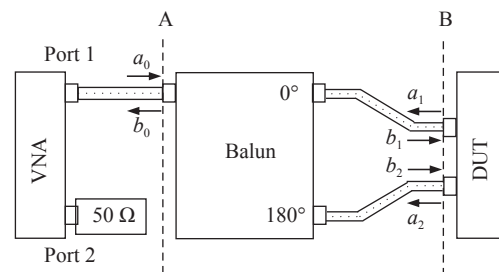


Figure 3 Setup for the balun method using a three-port 180° power divider.

short-open, short-load, short-short, match-open, match-match, match-short, open-open, open-match, open-short, and through, which can be realized by two VNA calibration kits. Third, one port of the VNA is connected to the input port of the balun, the other port of the VNA is terminated with a match load, and the one-port S -parameter from the VNA is measured ten times, each time with a different two-port standard on the output of the balun.

The balun and the output coaxial cables between reference planes A and B are represented by a three-port error network defined as a 3×3 S -parameter matrix:

$$\begin{bmatrix} b_0 \\ b_1 \\ b_2 \end{bmatrix} = \begin{bmatrix} e_{00} & e_{01} & e_{02} \\ e_{10} & e_{11} & e_{12} \\ e_{20} & e_{21} & e_{22} \end{bmatrix} \begin{bmatrix} a_0 \\ a_1 \\ a_2 \end{bmatrix} \quad (10)$$

where a_i and b_i are the incident and reflected voltage waves at reference planes A and B. The DUT or the calibration standard is characterized at reference plane B by a 2×2 S -parameter matrix:

$$\begin{bmatrix} a_1 \\ a_2 \end{bmatrix} = [S_a] \begin{bmatrix} b_1 \\ b_2 \end{bmatrix} \quad (11)$$

where S_a is known for a two-port standard but is to be known for the DUT. Equation (11) can be rearranged as

$$\begin{bmatrix} b_1 \\ b_2 \end{bmatrix} = [S_a]^{-1} \begin{bmatrix} a_1 \\ a_2 \end{bmatrix} = \begin{bmatrix} m_{11} & m_{21} \\ m_{12} & m_{22} \end{bmatrix} \begin{bmatrix} a_1 \\ a_2 \end{bmatrix} \quad (12)$$

The measurement made at reference plane A yields

$$b_0 = S_m a_0 \quad (13)$$

where S_m denotes the measured one-port raw S -parameter data. Due to the reciprocity of the balun and DUT, one can obtain $e_{01} = e_{10}$, $e_{02} = e_{20}$, $e_{21} = e_{12}$ in (10) and $m_{12} = m_{21}$ in (12), which leads to

$$\begin{bmatrix} m_{11} & m_{12} \\ m_{12} & m_{22} \end{bmatrix} = \begin{bmatrix} e_{11} - \frac{e_{01}^2}{e_{00} - S_m} & e_{12} - \frac{e_{02}e_{10}}{e_{00} - S_m} \\ e_{12} - \frac{e_{02}e_{10}}{e_{00} - S_m} & e_{22} - \frac{e_{02}^2}{e_{00} - S_m} \end{bmatrix} \quad (14)$$

The unknown e_{00} , e_{11} , e_{22} , e_{01}^2 , e_{02}^2 , e_{12} , e_{02} , and e_{10} can be solved from the above steps [43] through

$$S_m = e_{00} + \frac{\begin{bmatrix} (e_{01}^2 S_{a11} + e_{02}^2 S_{a22} + 2e_{01}e_{02}S_{a12}) \\ + (2e_{01}e_{02}e_{12} - e_{02}^2 e_{11} - e_{01}^2 e_{22})(S_{a11}S_{a22} - S_{a12}^2) \end{bmatrix}}{\Delta} \quad (15)$$

where

$$\Delta = 1 - S_{a11}e_{11} - S_{a22}e_{22} - 2e_{01}S_{a12} + (e_{11}e_{22} - e_{12}^2)(S_{a11}S_{a22} - S_{a12}^2) \quad (16)$$

The S -parameters of the DUT can be obtained as

$$[S_a] = \begin{bmatrix} S_{a11} & S_{a12} \\ S_{a21} & S_{a22} \end{bmatrix} = \begin{bmatrix} e_{11} - \frac{e_{01}^2}{e_{00} - S_m} & e_{12} - \frac{e_{02}e_{10}}{e_{00} - S_m} \\ e_{12} - \frac{e_{02}e_{10}}{e_{00} - S_m} & e_{22} - \frac{e_{02}^2}{e_{00} - S_m} \end{bmatrix}^{-1} \quad (17)$$

Finally, the input impedance of the DUT can be solved from

$$Z_{dif} = 2Z_0 \frac{1 - S_{a11}S_{a22} + S_{a12}S_{a21} - S_{a12} - S_{a21}}{(1 - S_{a11})(1 - S_{a22}) - S_{a21}S_{a12}} \quad (18)$$

Zhang and Tu also extended the calibration technique developed by Curry to remove the effects of the four-port 180° hybrid junction as the balun in differential antenna measurements. Interested readers are referred to [43], [44].

The balun method can not only measure the input impedance but also measure the radiation characteristics of the DUT simultaneously, which is particularly useful in evaluating impedance alterations as well as the radiation properties of differential antennas, such as due to proximity effects.

Antenna efficiency, an important antenna, is defined as the ratio of the power radiated by an antenna over the power delivered to the antenna. Pozar and Kaufman argued that direct measurement is often the only technique to reliably determine antenna efficiency because factors such as surface roughness, tolerance effects, and spurious radiation are difficult to account for in a theoretical calculation and can impose a drastic effect on the operating antenna efficiency [45].

According to the Wheeler method [46], if a differential antenna can be modeled by a series RLC circuit, its efficiency can then be calculated as

$$\eta = \frac{\text{Re}(Z_{dif}^{fs}) - \text{Re}(Z_{dif}^{wc})}{\text{Re}(Z_{dif}^{fs})} \quad (19)$$

If the differential antenna can be modeled by a parallel RLC circuit, its efficiency needs to be calculated as

$$\eta = \frac{\text{Re}(Z_{dif}^{wc}) - \text{Re}(Z_{dif}^{fs})}{\text{Re}(Z_{dif}^{wc})} \quad (20)$$

where $\text{Re}(Z_{dif}^{fs})$ and $\text{Re}(Z_{dif}^{wc})$ represent the real parts of the impedances of the differential antenna at the resonant frequency in free space and in a Wheeler cap, respectively [47].

The amplitude and phase imbalances of real baluns do not cause unacceptable errors in radiation pattern measurements [17]. It has been observed that the copolarization radiation patterns agree very well, despite the two baluns being different. The differences between the cross-polarization radiation patterns are quite weak and difficult to accurately measure. The insertion loss of the balun can be calibrated in the measurement of gain values of the differential antennas.

IV. Classification of Differential Antennas

There exist many differential antennas in either discrete or integrated forms, depending on their applications and design considerations. In this section, these are classified based on their construction and fabrication and examine their suitability.

1. Wire antennas

Metal wires are favorable conductors. Antennas such as dipole, loop, and Yagi-Uda are made of metal wires or rods. These are classified as differential wire antennas.

A dipole antenna commonly consists of two identical metal wires or rods. A loop antenna is usually made from a coil of metal wire. Dipole and loop antennas are the most basic antennas. A Yagi-Uda antenna is composed of three or more parallel metal rods. The Yagi-Uda antenna is a directional antenna radiating in the end-fire direction. The loop and dipole antennas can be connected in parallel to form a loop-dipole composite antenna. This is denoted as the Ω -shaped antenna or simply the Ω antenna [48].

Figure 4 shows the geometry of the Ω antenna and the coordinate system. The circular loop has a radius of a and is placed on the xoy plane with the center at the origin of the coordinate system. The circumference of the circular loop is C . The dipole has a length of $2l$ with its center tangential to the circular loop. The Ω antenna comprises metal wire with radius b .

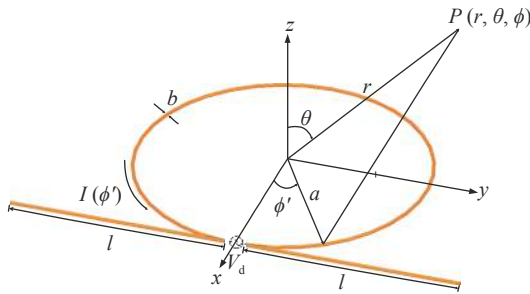


Figure 4 Geometry of the Ω antenna and the coordinate system.

Under the thin-wire approximation of $b \ll \lambda$, Fang and Zhang have recently analyzed the Ω antenna driven by a delta-function source of voltage V . When considering the circular loop antenna, they first validated Storer's theory for the current distribution along the circumference of a circular loop antenna as a Fourier series and the analytical solution to the input impedance [49] and then confirmed the extension of Storer's theory for the radiation characteristics of the circular loop antenna by Rao [50]. When considering dipole antenna, they adopted the sinusoidal current distribution along the length of the dipole antenna. However, they did not use the available expressions for the radiated fields directly because the location of the dipole antenna in the Ω antenna was different from that of the normal single dipole antenna in the coordinate system. Instead, they had to derive the radiation characteristics, as given by

$$\begin{aligned}
 E_{\theta}^{\Omega} &= E_{\theta}^L + E_{\theta}^D \\
 &= \frac{jk_0 a V_d}{\pi} \frac{e^{-jk_0 r}}{r} \sum_{n=1}^4 \frac{j^n}{\alpha_n} \frac{n J_n(k_0 a \sin \theta) \cos \theta}{k_0 a \sin \theta} \sin(n\phi) \\
 &\quad - \frac{j\eta_0 I_m}{4\pi} \frac{e^{-jk_0 r}}{r} e^{jk_0 a \sin \theta \cos \phi} \{\Theta\} \cos \theta \sin \phi \\
 \Theta &= \frac{\cos(k_0 l \sin \theta \sin \phi) - \cos[\beta l - k_0 \delta(n_1 + \sin \theta \sin \phi)]}{n_1 + \sin \theta \sin \phi} \\
 &\quad + \frac{\cos(k_0 l \sin \theta \sin \phi) - \cos[\beta l - k_0 \delta(n_1 - \sin \theta \sin \phi)]}{n_1 - \sin \theta \sin \phi}
 \end{aligned} \tag{21}$$

$$\begin{aligned}
 E_{\phi}^{\Omega} &= E_{\phi}^L + E_{\phi}^D \\
 &= \frac{jk_0 a V_d}{\pi} \frac{e^{-jk_0 r}}{r} \sum_{n=1}^4 \frac{j^n}{\alpha_n} \frac{n J_n(k_0 a \sin \theta) \cos \theta}{k_0 a \sin \theta} \sin(n\phi) \\
 &\quad - \frac{j\eta_0 I_m}{4\pi} \frac{e^{-jk_0 r}}{r} e^{jk_0 a \sin \theta \cos \phi} \{\Theta\} \cos \theta \sin \phi
 \end{aligned} \tag{22}$$

where α_n is the coefficient for the Fourier series [49], δ is the half gap for the delta-function source, n_1 is the wave-length shortening factor [51], $\beta = n_1 k_0$, and

$$I_m = \frac{V_d}{Z_{\text{dif}}^D \sin \beta(l - \delta)} \tag{23}$$

In (23), Z_{dif}^D , the input impedance of the dipole antenna, can be expressed as

$$Z_{\text{dif}}^D = Z_b \left(1 - j \frac{\alpha}{\beta} \right) \frac{\text{sh}(2\alpha l) - j \sin(2\beta l)}{\text{ch}(2\alpha l) - \cos(2\beta l)} \tag{24}$$

where

$$Z_b = 120 \left[\ln \left(\frac{2l}{b} - 1 \right) \right] \tag{25}$$

$$\alpha = \frac{R_r}{Z_b l \left[1 - \frac{\sin(2\beta l)}{2\beta l} \right]} \tag{26}$$

In (26), R_r can be expressed as

$$R_r = \frac{15}{2\pi} \int_0^{2\pi} \int_0^{\pi} (1 - \sin^2 \theta \sin^2 \phi) [A(\theta, \phi) + B(\theta, \phi)]^2 \sin \theta d\theta d\phi \tag{27}$$

where

$$A(\theta, \phi) = \frac{\cos(k_0 l \sin \theta \sin \phi) - \cos[\beta l - k_0 \delta(n_1 + \sin \theta \sin \phi)]}{n_1 + \sin \theta \sin \phi} \tag{28}$$

$$B(\theta, \phi) = \frac{\cos(k_0 l \sin \theta \sin \phi) - \cos[\beta l - k_0 \delta(n_1 - \sin \theta \sin \phi)]}{n_1 - \sin \theta \sin \phi} \tag{29}$$

Hence, the input impedance of the Ω antenna can be obtained as

$$Z_{\text{dif}}^{\Omega} = \frac{Z_{\text{dif}}^L Z_{\text{dif}}^D}{Z_{\text{dif}}^L + Z_{\text{dif}}^D} \quad (30)$$

where Z_{dif}^L , the input impedance of the circular loop antenna, is given in [49].

Figure 5 shows the simulated current distribution for the Ω antenna with C and $2l$ representing half the free-space wavelength. It is evident that the current is mainly concentrated on the dipole. Therefore, the radiation of the Ω antenna is similar to that of the dipole antenna, as shown in Figure 6. The current on the circular loop affects the cross-polarization of the yo z plane.

Figure 7 shows the calculated and simulated input impedances. Note that the agreement between them is good.

The slight discrepancies exist because conductor losses and terminal effects have been neglected in the theory [47].

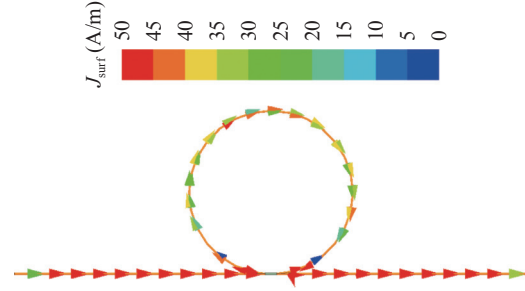


Figure 5 Current distribution on the Ω antenna at 3 GHz.

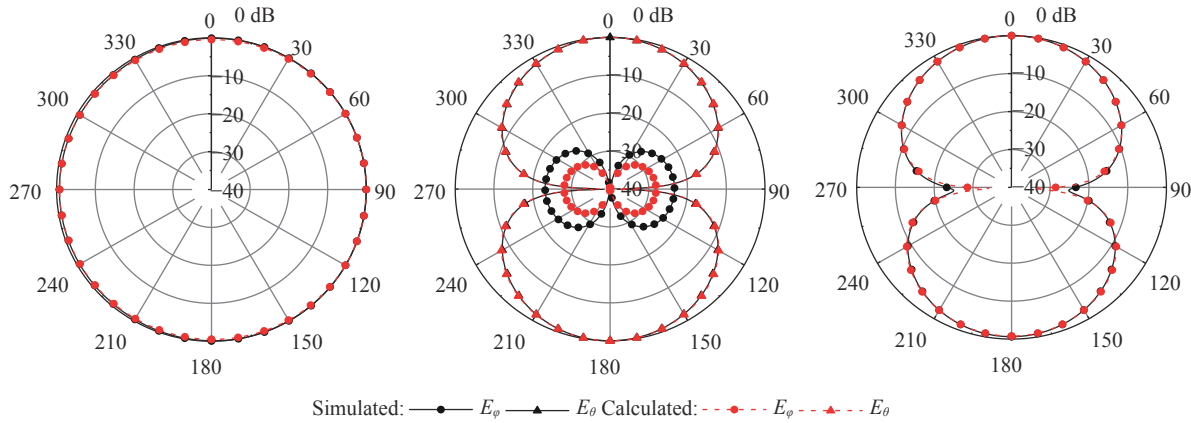


Figure 6 Calculated and simulated radiation patterns of the Ω antenna on the xoz , yo z, and xoy planes at 3 GHz.

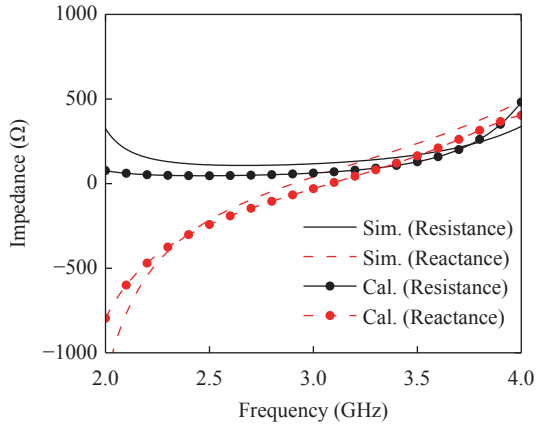


Figure 7 Calculated and simulated input impedance of the Ω antenna.

2. Slot antennas

A slot antenna is cut into a flat metal sheet. As its currents are not confined to the edges of the slot but spread out over the sheet, the slot antenna is an efficient radiator. Radiation propagates equally from both sides of the sheet [10]. The rectangular slot is the most popular slot shape for antennas. Other slot shapes, such as dumbbell and triangular slots, can also be found.

Slot and dipole antennas are complementary. Let Z_{dif}^D

and Z_{dif}^S represent the differential input impedances of the dipole and slot antennas that are cut from an infinitesimally thin, perfectly conducting, and infinitely large plane; these are linked by Booker's relation [52] as

$$Z_{\text{dif}}^D Z_{\text{dif}}^S = \frac{\eta_0^2}{4} \quad (31)$$

where η_0 , the intrinsic impedance of free space, is equal to $120\pi \Omega$.

The single-ended input impedance of the monopole antenna is $Z_{\text{sig}}^m = Z_{\text{dif}}^D/2$. Though the half slot is still a half-wavelength slot antenna, it can be considered as a single-ended antenna with the input impedance $Z_{\text{sig}}^{\text{hs}} = Z_{\text{dif}}^S/2$. Thus, one can obtain a new impedance relation for the single-ended monopole and half-slot antennas as

$$Z_{\text{sig}}^m Z_{\text{sig}}^{\text{hs}} = \frac{\eta_0^2}{16} \quad (32)$$

Similarly, one can also find another new useful impedance relation for the single-ended monopole and differential full slot antennas as follows:

$$Z_{\text{sig}}^m Z_{\text{dif}}^S = \frac{\eta_0^2}{8} \quad (33)$$

3. Microstrip antennas

A microstrip antenna consists of a very thin metallic strip of various shapes on a grounded dielectric substrate. Interestingly, the first microstrip antenna was a differential disk antenna published by Byron in 1970 [9]. The microstrip antenna concept aroused the attention of the antenna community, mainly due to the works of Munson and Howell between 1972 to 1974 [53]–[56]. Munson's work showed microstrip antennas as a practical concept for solving many antenna system problems, giving birth to a new antenna industry [57].

Byron, Howell, and Munson's works on microstrip antennas invigorated the antenna community. Soon, an avalanche of papers and books followed on microstrip antennas, which by the 1980s was reaching maturity and has been continually developed in the antenna field for over half a century. Compared with the many papers on single-ended microstrip antennas, there were few papers on differential microstrip antennas in the 1980s [58]–[62], despite the latter having clearly shown advantage in suppressing higher-order modes, reducing cross-polarized radiation, removing pattern distortion, and producing an improved axial ratio for circular polarization.

For the microstrip patch antenna, the differential impedance Z_{dif} can be expressed [37] as

$$Z_{\text{dif}} = 2 \sum_{m,n=0}^{\infty} (Z_{11,mn} - Z_{12,mn}) = 4 \sum_{m=0, n=2i+1}^{\infty} Z_{11,mn} \quad (34)$$

where $Z_{11,mn}$ is the mode impedance on port 1 for the m th mode, $Z_{12,mn}$ is the mode impedance between ports 1 and 2 for the m th mode, $i = 0, 1, 2, 3, \dots$. It is important to note that Z_{dif} has no term of n being an even number. The single-ended impedance Z_{sig} can be expressed [37] as

$$Z_{\text{sig}} = \sum_{m=0}^{\infty} \sum_{n=0}^{\infty} Z_{11mn} \quad (35)$$

Note that Z_{sig} contains terms regardless of whether n is an odd or even number. Thus, the ratio of Z_{dif} to Z_{sig} is

$$\frac{Z_{\text{dif}}}{Z_{\text{sig}}} = 4 \left(\sum_{m=0}^{\infty} \sum_{n=2i+1}^{\infty} Z_{11mn} \right) \left(\sum_{m=0}^{\infty} \sum_{n=0}^{\infty} Z_{11mn} \right)^{-1} \approx 4 \quad (36)$$

Additionally, it should be mentioned that the patch size in the above derivation remains the same for both differential and single-ended operations [37], [63]. Hence, the size ratio is 1. The electrical separation is defined as the ratio of the physical distance between the dual feeds over the free-space wavelength. It plays an important role in the design of a differential microstrip patch antenna. It has been found that the electrical separation needs to be larger than 0.1 to guarantee the fundamental resonance [12], [20].

The stacked microstrip patch antenna was first reported by Hall, Wood, and Garrett in 1979 for broadband operation [64]. Since then, it has been quite popular because it not only delivers a wide impedance bandwidth but also pro-

vides additional electrical, mechanical, and thermal advantages. Shao *et al.* reported the design and optimization of differential stacked microstrip patch antennas using the Bat algorithm [65]. They considered the stacked microstrip patch antenna as two stacked microstrip lines. Then, they applied quasieven and odd modes to provide new insight into the resonance, coupling, and radiation of the stacked microstrip patch antenna. For the even mode, the charges are equal on both the upper and lower patches, which results in a weak electric field distribution between the patches but a strong electric field distribution between the lower patch and the ground plane. In contrast, the charges oppose each other on both the upper and lower patches for the odd mode, which results in a strong electric field distribution between the patches but a weak electric field distribution between the lower patch and the ground plane. The even mode produces in-phase currents on both the upper and lower patches, while the odd mode produces out-of-phase currents on the two patches. The in-phase currents enhance radiation, while the out-of-phase currents weaken radiation.

The shorted microstrip patch antenna was derived from the microstrip patch antenna by Garvin *et al.* They reported a missile base mounted SPA in 1977 [66]. The shorted microstrip patch antenna is harder to design for differential operation due to its structure as a quarter-wavelength antenna. To create a differential shorted microstrip patch antenna (DSPA) from a single-ended shorted microstrip patch antenna (SPA), Shao and Zhang first cut a narrow gap g along the centerline perpendicular to the shorting edge; then, they moved the half-shortening wall to the opposite edge and added an extra feed to the patch [24]. This work demonstrated that the novel DSPA can be smaller than a normal SPA at the same resonant frequency. The extent of size reduction of the DSPA is determined by the gap coupling effect. A coupled transmission-line model has been developed to predict the resonance of the DSPA and succinctly provide deep physical insight. It has been revealed that, except for gap width, the coupling is dominated by the patch ratio and substrate thickness rather than the dielectric constant. In addition, the DSPA shows a comparable or narrower impedance bandwidth, higher directivity, lower radiation efficiency, more symmetrical radiation patterns, and lower cross-polarization radiation than the SPA.

The planar inverted-F antenna (PIFA) was first reported by Taga and Tsunekawa in 1987 [67]. The PIFA can be viewed as evolved from the SPA but with a smaller size. Hence, the PIFA is quite popular in portable antenna design. Shao and Zhang reported the differential PIFA (DPIFA) [23] in 2019. They described the frequency trimming and, more importantly, the miniaturization of the DPIFA. They derived a simple formula for determining the resonant frequency of a DPIFA. They have shown that the DPIFA provides better performance than the PIFA. More importantly, the size of the DPIFA is smaller than that of the PIFA for a given resonant frequency.

The grid array antenna was invented by Kraus in 1962

as a traveling-wave (nonresonant) antenna with the main lobe of radiation in a backward angle-fire direction [68]. The grid array antenna was implemented in microstrip technology by Conti *et al.* in 1981 as a standing-wave (resonant) antenna with the main beam of radiation in the broadside direction [69]. Kraus proposed a differential feeding technique that used two wires passing through one opening in the ground plane to connect the source with the opened center of the radiating element. Zhang *et al.* proposed another differential feeding technique [28] that used two coaxial probes with outer conductors connected to the ground plane and inner conductors connected to the two ends of the radiating element. The novel feeding technique avoided opening the radiating element and resulted in a large physical separation between the two feeding points that eased the testing procedure. The separation can be half guided wavelength or farther apart, such as with one and a half- or two-handed half guided wavelengths.

Figure 8 displays the simulated current distributions on the microstrip grid array antenna under parallel resonance. The current distribution by the usual differential excitation concentrates on the radiating elements near the feeding points, indicating a low aperture efficiency. The current distribution was improved by the novel differential excitation [28]. As a result, the impedance matching, gain, and gain bandwidth were enhanced. The enhancement is mainly attributed to the novel placement of dual coaxial probes, which help to maintain current phase synchronization on the radiating elements. It was found that the currents are only truly out-of-phase on the long sides and are in-phase on

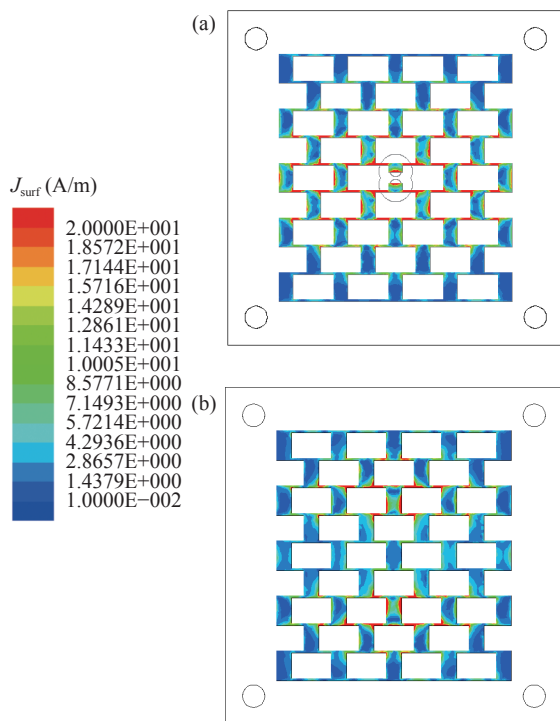


Figure 8 Simulated current distributions: (a) The usual and (b) novel differential excitations.

the short sides of the loops (near the feeding point) because at such a high frequency, a slight loop dimension change would induce a big change in signal phase over transmission. Thus, control over phase synchronization of the loops far from the feed point would be much more difficult to achieve. The conventional placement of the twin wires in [68] could be similarly to the placement of a single feed and shows poorer performance due to not improving current phase synchronization.

4. Printed antennas

A printed antenna is an antenna printed on one surface of a dielectric substrate with no ground plane existing directly underneath the radiator on the other surface. The absence of the ground plane directly underneath the radiator makes the printed antenna radically different from the microstrip antenna. The quasi-Yagi, fractal, and spiral antennas are typical printed antennas for end-fire radiation, multiband, and wideband operations, respectively.

The quasi-Yagi antenna was first reported by Qian *et al.* in 1998 as a single-ended antenna, although the driver is differential [70]. Recently, Zhu and Zhang modified it to a differential quasi-Yagi antenna [71]. Figure 9 shows the simulated electric field distributions on the top and bottom surfaces of the differential quasi-Yagi antenna printed on a substrate with a dielectric constant of 10.2 and a thickness of 0.635 mm at X-band frequencies. As expected, the surface wave of the TE_0 mode is indeed strongly excited and propagated in the directions normal to the driver. Since the polarization direction of the electric field on the driver is

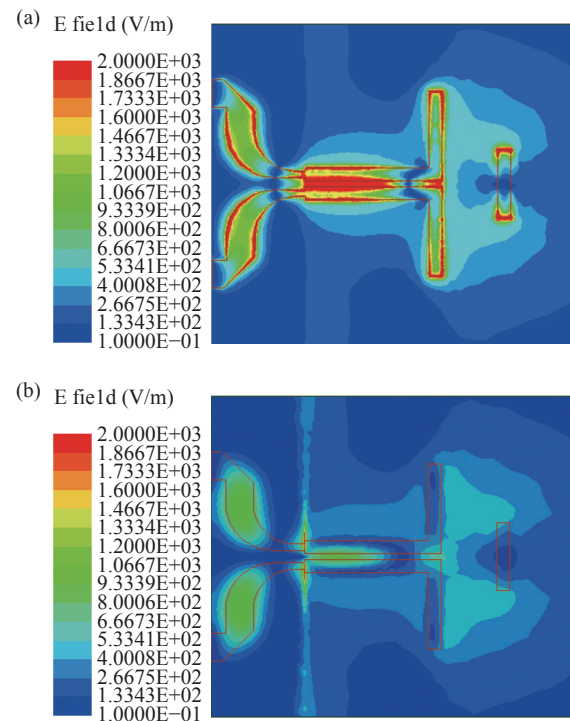


Figure 9 Simulated electric field distributions: (a) top and (b) bottom surfaces of the printed differential quasi-Yagi antenna.

the same as that of the electric field on the director, there will be strong coupling between them. Therefore, the surface wave of the TE_0 mode is guided to radiate in the end-fire direction. However, due to the existence of the ground plane or the reflector, the surface wave of the TE_0 mode cannot be propagated in the grounded substrate region and will be reflected back, further strengthening the radiation in the end-fire direction. It should be noted that the surface wave of the TM_0 mode is quite weakly excited, and can propagate along the axial directions of the driver in both the grounded and ungrounded substrate regions. This causes cross-polarized radiation and deteriorates the antenna gain and front-to-back ratio. Therefore, in designing the quasi-Yagi antenna, a major concern is how to excite the surface waves of the TE_0 mode to the greatest extent and the surface waves of the TM_0 mode to the lowest extent.

Figure 10 shows the simulated and measured radiation patterns in the E-plane at 8.2 GHz. The patterns are normalized with the maximum of 0 dB. The measured co- and cross-polarized radiation patterns are in the solid and dot-dashed lines, respectively, while the simulated co- and cross-polarized radiation patterns are in the dashed and dot lines, respectively.

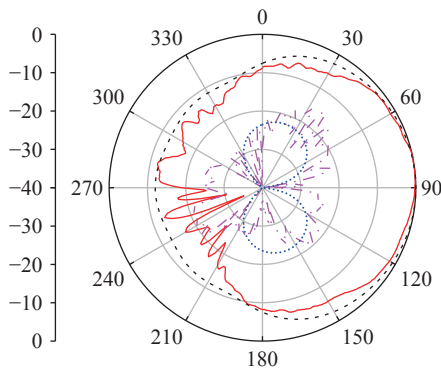


Figure 10 Simulated and measured patterns of the differential quasi-Yagi antenna.

The fractal antenna uses a fractal, self-similar design for multiband operation. Puente *et al.* introduced the Sierpinski gasket monopole as a single-ended printed multiband antenna in 1996 [72]. Recently, Fang and Zhang modified it to a differential fractal antenna [73]. Figure 11 shows the simulated current density distributions on half of the differential fractal antenna printed on a substrate with a dielectric constant of 2.2 and a thickness of 1.588 mm at the resonant frequencies [73]. The right column presents an expanded view of the region where most of the current is concentrated at each frequency. The scale factor of two is the same as that existing among the bands. The most interesting feature of such plots is that the current density distributions are very similar. This becomes especially apparent when neglecting the effect of the smaller holes at the lower bands. Figure 12 shows the simulated and measured $|S_{d11}|$ of the printed differential fractal antenna as a function of frequency. It is evident that the printed differential fractal

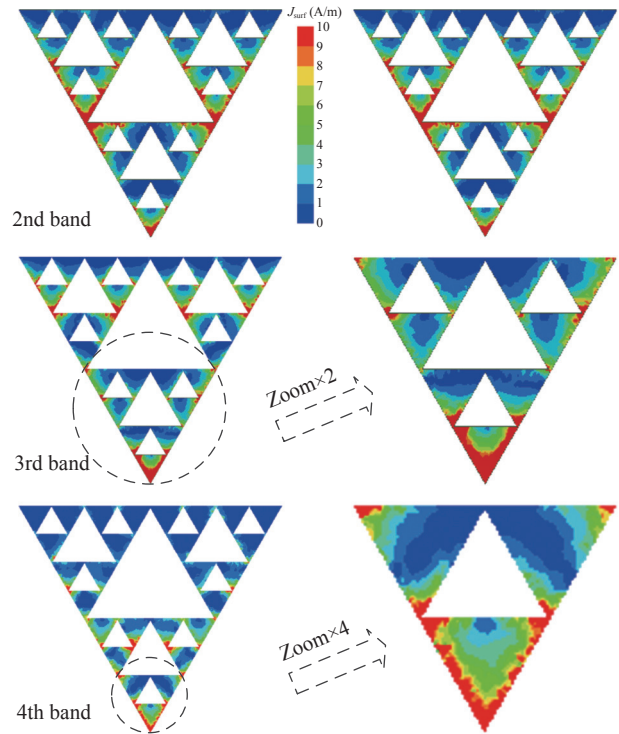


Figure 11 Simulated current density distributions on half of the printed differential fractal antenna at the resonant frequencies. The left column displays the whole antenna at the three upper bands, while the right column shows a zoomed view of the active region at each band.

antenna can operate in the four bands at 0.65, 2.00, 4.00, and 8.00 GHz, respectively.

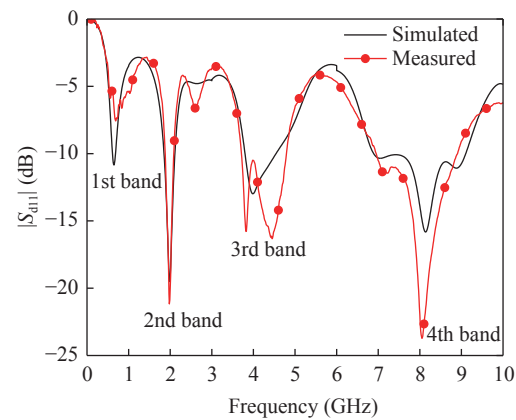


Figure 12 Simulated and measured $|S_{d11}|$ of the printed differential fractal antenna as a function of frequency.

It is desirable that an antenna demonstrate the ability to radiate efficiently over a wide frequency bandwidth. Rumsey conceived the idea of frequency-independent antennas in the early 1950s, which revealed that the impedance and radiation pattern properties of an antenna are frequency independent if the antenna shape is specified only in terms of angles [74]. Rumsey's concept was implemented experimentally by Dyson, who constructed the first planar equiangular spiral antenna cut out of a metal sheet [7]. Figure 13 shows the simulated current distribution on the

spiral antenna printed on a substrate with a dielectric constant of 6.15 and a thickness of 1.27 mm at the central frequency of the wideband from 1 to 6 GHz [75].

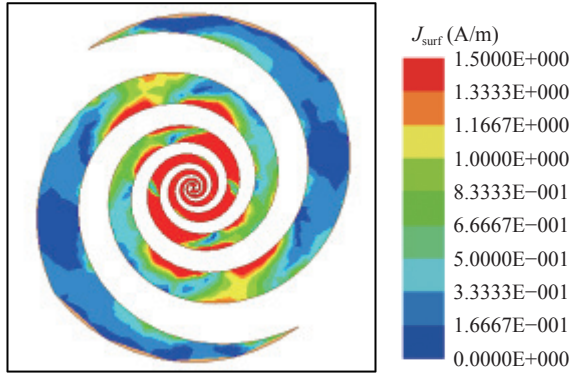


Figure 13 Simulated current density distribution on the printed differential spiral antenna at the central frequency of the wideband from 1 to 6 GHz.

Figure 14 shows the simulated input impedance of the printed differential spiral antenna. As shown, a nearly constant impedance of 100 Ω can be seen over the frequency band from 1 to 5 GHz. This is an expected behavior of a frequency-independent antenna. The frequency band from 1 to 5 GHz is referred to as the “operating band.” Since the printed differential spiral antenna is a quasiself-complementary antenna, its input impedance can be estimated by Mushiake’s relation [76] as

$$Z_{\text{dif}} = \frac{\eta_0}{2\sqrt{\frac{\epsilon_r + 1}{2}}} = \frac{120\pi}{2\sqrt{\frac{6.15 + 1}{2}}} \approx 100 \Omega \quad (37)$$

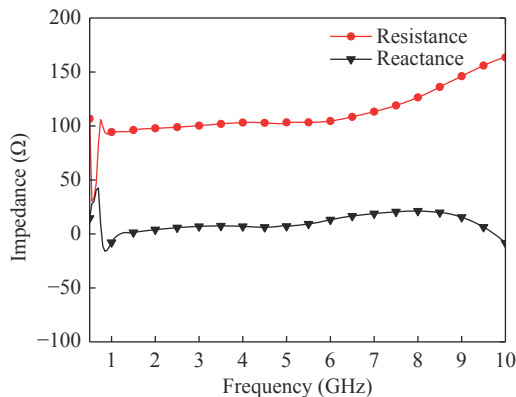


Figure 14 Simulated and measured impedance of the printed differential spiral antenna as a function of frequency.

5. Dielectric resonator antennas

A dielectric resonator antenna is a block of dielectric material that can take various shapes. Long *et al.* reported the first design and test of dielectric resonator antennas in 1983 [10]. They showed that dielectric resonator antennas present inherent advantages of small size, low loss, and relatively wide bandwidth.

Leung and colleagues have conducted intensive and extensive studies of dielectric resonator antennas since the early 1990s [77]. They reported the first differential dielectric resonator antenna in 2008 [78], which was a rectangular dielectric resonator antenna excited in its fundamental broadside mode. They realized a compact differential hollow dielectric resonator antenna in 2010 [79], a differential dielectric resonator antenna loaded with chip varactors for frequency tunability in 2011 [80], and a differential dielectric resonator antenna array in 2018 [81].

Tang *et al.* extended the design of differential dielectric resonator antennas for dual-band and dual-polarized operation [82], [83] and for integration with filters [84]. More interestingly, they developed a substrate-integrated differential cavity-backed dual-polarized dielectric resonator antenna with a wide bandwidth, low profile, high isolation, and improved gain [85]. Tian *et al.* combined the functions of the duplexer, the filter, and the antenna into one highly integrated differential module for common-mode suppression [86].

Dielectric resonator antennas offer no inherent conductor loss, which is especially attractive for millimeter-wave (mmWave) antennas, where the loss in metal fabricated antennas can be high. Chen *et al.* developed a differential dual-polarized 2-D multibeam dielectric resonator antenna array based on a printed ridge gap waveguide [87]. The measured results show an impedance bandwidth of 10% (28.5–31.5 GHz) and a peak gain of 11.8 dBi. Additionally, the measured cross-polarization discrimination is 28.3 dB at the center frequency and larger than 19.2 dB over the band of operation. In addition, a measured radiation efficiency of 67% is achieved for both polarizations at 30 GHz.

V. Applications of Differential Antennas

Differential antennas have found applications in radios, radars, imagers, sensors, etc. This section provides typical application examples of differential antennas from simple discrete wire to sophisticated integrated designs in antenna-in-package (AiP) or antenna-on-chip (AoC) technologies.

1. Television

The Yagi-Uda antenna is relatively lightweight, inexpensive, and simple to construct. It radiates linearly polarized radio waves with a gain of up to 20 dBi. Its largest and best-known use is as a rooftop television antenna.

2. Bluetooth radio

Bluetooth radio is a wireless technology standard for personal area networks. It is implemented in CMOS technology as a wireless SoC operating from 2.402 GHz to 2.48 GHz. Figure 15 shows a photo of the top and bottom views of a cavity-down ball grid array package in low-temperature co-fired ceramic (LTCC) technology. The package has dimensions of $15 \times 15 \times 1.6 \text{ mm}^3$. It integrates a differential microstrip patch antenna on the top surface and can carry a Bluetooth radio SoC die in the cavity to realize an AiP module.

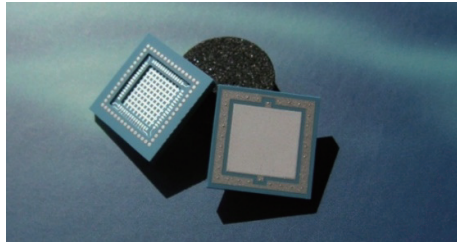


Figure 15 Differential microstrip patch antenna in AiP for Bluetooth radio.

3. Wi-Fi radio

Wi-Fi radio is a family of wireless technology standards for local area networks. Wi-Fi radio is also implemented in CMOS technology as a wireless SoC operating at 2.4, 5, and 6 GHz. Figure 16 shows the photo of the top and bottom views of a cavity-down ball grid array package in the LTCC technology. The package has a size of $17 \times 17 \times 1.6$ mm³. It integrates a differential microstrip line antenna on the top surface and can carry a Wi-Fi radio SoC die in the cavity to realize an AiP module.

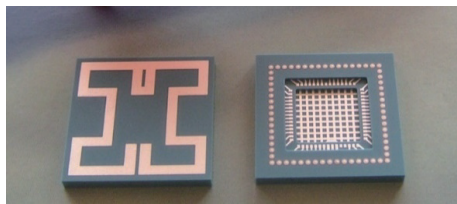


Figure 16 Differential microstrip patch antenna in AiP for Wi-Fi radio.

4. Ultrawideband radio

Ultrawideband (UWB) radio is a wireless technology standard with a fractional bandwidth greater than 20% or a bandwidth greater than 500 MHz. UWB radio allows for the transmission of a large amount of data at a very low energy level without interfering with conventional narrowband and carrier wave transmission in the same frequency band. Figure 17 shows a photo of a printed differential spiral antenna for UWB radio. It has a size of $50 \times 50 \times 25$ mm³. The impedance bandwidth ranges from 2.4 to 5.8 GHz. The gain values are 3.5 dBi over the bandwidth [88].

5. New radio

The New Radio (NR) is a new radio access technology developed by third Generation Partnership Project (3GPP) for the 5G (fifth generation) mobile network. Figure 18 shows a photo of the world's first fully integrated mmWave AiP module for 5G NR smartphones and mobile devices. The AiP integrates stacked microstrip patch antennas for broadside radiation and dipole antennas for end-fire radiation [89].

6. 60-GHz radio

To provide a multiple gigabit wireless system standard, 60-GHz radio has been developed. Figure 19 shows the photo of the top and bottom views of 60-GHz CMOS radio SoC integrated with a four-element AiP that addresses the chal-



Figure 17 Printed differential antenna for UWB radio.



Figure 18 Differential dipole antenna array in an AiP for 5G NR at 28 GHz.

lenge of omni-directional operation in the 60-GHz band using a switched-beam approach to enable broad angular coverage [90]. The AiP has a size of $11 \times 11 \times 0.5$ mm³ that supports the differential transmit and single-ended receive paths in both broadside and end-fire directions with four antennas. Both single-ended and differential patch antennas are used for the broadside direction, while both single-ended and differential quasi-Yagi antennas are used for the end-fire direction. Note that the driver is a folded dipole rather than the ordinary dipole. This design facilitates the impedance matching between the driver and coplanar strip lines from the manufacturable point of view. The simulated antenna peak gains are 4.3 and 5.1 dBi for the differential and single-ended quasi-Yagi antennas, respectively. The simulated impedance bandwidth is at least 4 GHz for both differential and single-ended quasi-Yagi antennas. Another AiP with the integrated differential quasi-Yagi antenna for 60-GHz radio can be found in [91].

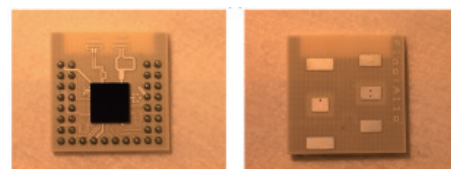


Figure 19 Differential microstrip patch and quasi-Yagi antenna in an AiP for 60-GHz radio.

7. Gesture radar

Gesture radar can comprehend human motion at various scales and has gained increasing attention in recent years, as driven by the growth of virtual reality (VR) and augmented reality (AR). Figure 20 shows the micrograph of the top and

bottom views of a 60-GHz gesture radar in an AiP [92]. It was developed on the embedded wafer level ball grid array (eWLB) technology with a size of $14 \times 14 \times 0.8 \text{ mm}^3$ and integrates two differential microstrip patch antennas for transmission and four single-ended rectangular microstrip patch antennas for reception. The differential microstrip patch antenna was fed by two microstrip transmission lines. To reduce the electrical separation, a slit was cut on the patch between the two feeding lines. The simulated results showed a gain of 4 dBi and a bandwidth of approximately 15 GHz at 60 GHz.

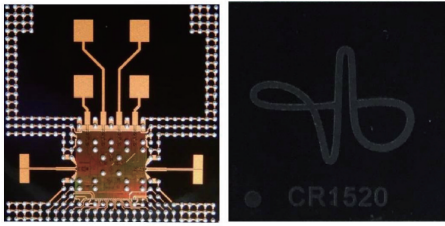


Figure 20 Differential microstrip patch antennas in an AiP for 60-GHz gesture radar.

8. Automotive radar

Automotive radars operate in the frequency band between 77–81 GHz for medium-range and short-range applications, such as collision warning, blind spot detection, and pre-crash vehicle preparation. The rapid development of highly integrated multichannel transceiver chips in silicon germanium (SiGe) or CMOS technologies enables the realization of compact and low-cost radars, which are a prerequisite for mass-market adoption. Compared to traditional soft substrate materials, radar sensors based on LTCC offer better mechanical stability and higher thermal conductivity. **Figure 21** shows the photo of the top and bottom views of a short-range radar sensor built using a four-channel fully differential transceiver chip in SiGe technology and four single-row and four double-row microstrip grid array antennas in LTCC technology [93]. The compact radar module has a size of $23 \times 23 \times 1.416 \text{ mm}^3$. The microstrip grid array antennas were fed differentially with laminated waveguides. The measured 3-dB beamwidth at 79 GHz for a single row is 16° in the E-plane and 58° in the H-plane. The measured 3-dB beamwidth at 79 GHz for a double row is 16.5° in the E-plane and 40° in the H-plane. The calibrated measured gain is 12.4 dBi for the single-row antenna and 14 dBi for the double-row grid antenna.

9. 160-GHz sensor

Industrial and life science applications often require sensors with special functionality, smaller size, lower power consumption, higher accuracy, easier applicability, and broader imaging capabilities. **Figure 22** shows a micrograph of the fabricated 160-GHz sensor for food scanning [94]. It integrates a differential microstrip grid array antenna on the copper redistribution layer with the chip in a $6 \times 6 \text{ mm}^2$ eWLB package.

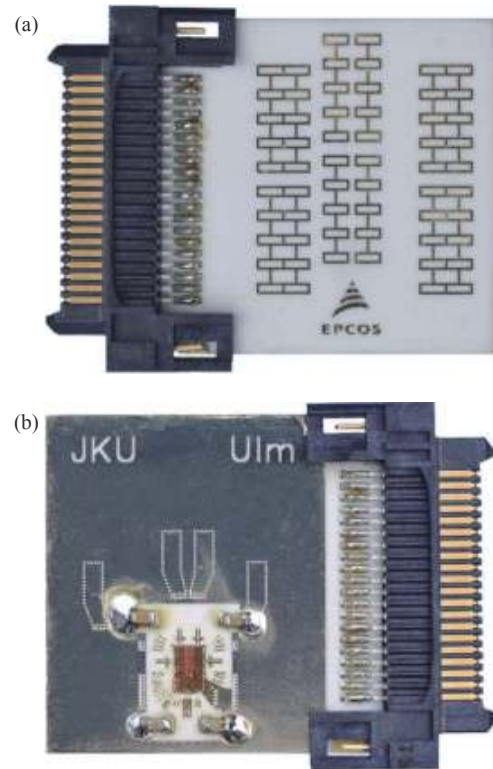


Figure 21 Differential microstrip grid array antennas in an AiP for 79-GHz automotive radar: (a) top and (b) bottom surfaces.

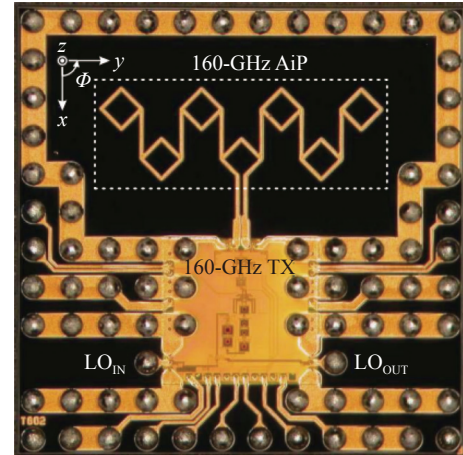


Figure 22 Differential microstrip grid array antennas in an AiP for a 160-GHz sensor.

10. 300-GHz array

The 300 GHz band offers the potential to achieve significantly higher transmission rates than conventional wireless communications. It has been identified as a candidate band for future wireless communications. **Figure 23** shows the micrograph of a 300-GHz wirelessly locked 2×3 array radiating 5.4 dBm with 5.1% DC-to-RF efficiency in 65 nm CMOS [95]. The array integrates differential loop antennas and occupies an area of $1.1 \times 2.0 \text{ mm}^2$.

11. 650-GHz imager

There is substantial interest in terahertz (THz) technology

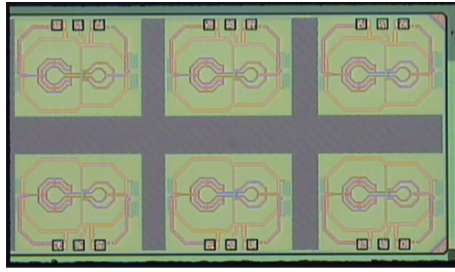


Figure 23 Differential loop antennas in an AoC for 300 GHz.

across various scientific disciplines. **Figure 24** shows a chip in 0.25 μm CMOS technology. It integrates 15 differential microstrip patch antennas for imaging at 0.65 THz [96]. The microstrip patch of size $88 \times 100 \mu\text{m}^2$ was separated 8 μm from the ground plane and connected to the detector through two 130- μm -long microstrip transmission lines. The simulated results showed a gain of 2.1 dBi and a bandwidth of approximately 15 GHz.

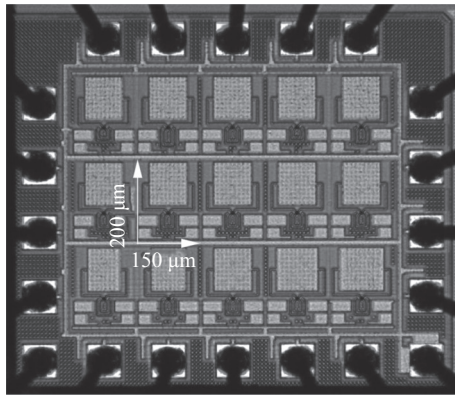


Figure 24 Differential microstrip patch antennas in an AoC for a 650-GHz imager.

12. RF energy harvester

RF energy harvesting converts energy from ambient electromagnetic waves emitted from widespread RF transmitters (such as indoor Wi-Fi routers and outdoor base stations) into DC voltages. A basic RF energy harvester consists of an antenna and a rectifying circuit. Its antenna requires a wide beam and high gain. With one antenna port, the gain and beamwidth always conflict. Thus, a multipoint antenna that uses the same antenna aperture for multiple beams could present a promising solution for RF energy harvesting. The multipoint and multibeam antenna could be equivalent to multiple antennas of different high-gain beams. Hu *et al.* proposed using a differential microstrip grid array antenna to implement this idea [97], as shown in **Figure 25**.

13. Biomedical monitor

An ingestible wireless capsule for endoscopy diagnosis requires an antenna for setting up a wireless data link from the ingestible capsule to the external receiver [98]. **Figure 26** shows an electrically small differential loop antenna with complex impedance for this application. The antenna's top

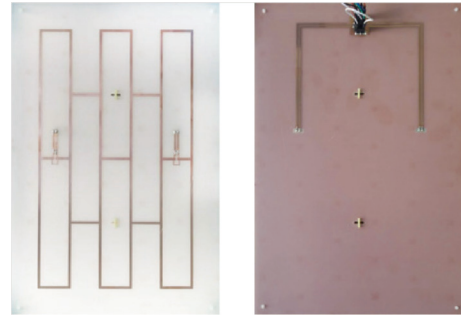


Figure 25 Differential microstrip grid array antennas for the RF energy harvester.

layer consists of an electrically small loop and an adjacent meandered radiator. In addition, an additional radiator is implemented on the antenna's bottom layer to enhance the bandwidth.

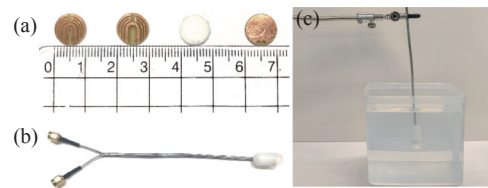


Figure 26 Differential loop antenna for ingestible wireless capsules: (a) fabricated in each layer, (b) antenna connected with a two-port test fixture, and (c) antenna placed inside the muscle phantom for measurement.

14. Internet of things device

The Internet of Things (IoT) is an emerging enabler of communication between people and/or devices. It will change our lives by creating new dimensions of an interconnected world. **Figure 27** shows a photo of an IoT device with a printed differential dipole antenna that can operate at 915 MHz [99].



Figure 27 Differential dipole antenna for IoT device.

VI. Conclusions

In the past, wireless systems such as radios and radars were implemented with discrete components. There existed a clear boundary between the circuit and antenna worlds and there was limited collaboration between the circuit and antenna communities. Therefore, different technical terms de-

veloped, such as the circuit community denoting devices as differential and single-ended circuits, whereas the antenna community denoted them as balanced and unbalanced antennas. Although some antenna researchers have realized that characterizing antennas by their structures as balanced or unbalanced might cause confusion, these old terms remain used in practice today. At present and into the future, the design of wireless systems from antennas to integrated circuits follows the trend of high integration. There is no longer a clear boundary between the circuit and antenna communities. Therefore, it is opportune to distinguish antennas by their sources as differential and single-ended antennas. This paper advocates to adopt these new terms of differential and single-ended antennas because the code-sign and joint integration of antennas and circuits for the modern RF SoC or SiP module has generated the need to co-optimize antennas and circuits within a circuit simulator relying on extracted compact models of antennas from an electromagnetic solver. The historic relationship between a differential antenna and its single-ended counterpart has been well characterized by image theory. The new relationship between another differential antenna and its single-ended counterparts was proven by the fact that they device show the same complex power as the antennas. The foregoing relationships are important and useful because the properties of either differential or single-ended antennas can be determined from the properties of the counterpart device with a known solution. Relatedly, we made a comparison of three methods for differential antenna measurements. Special emphasis was given to the balun method because it can not only measure the input impedance but also measure the radiation characteristics of the differential antenna simultaneously. It was further shown that removal balun effects is quite complicated. The classification of differential antennas into different types helped to describe the suitability of each antenna type more clearly. Five types of differential antennas were examined from simple discrete wire antennas to sophisticated integrated microstrip antennas. A new differential wire antenna, the Ω antenna, was analyzed. The creation of a differential shorted microstrip patch and planar inverted-F antennas was discussed with a focus on the capacitive coupling between the two structural halves or the electric coupling between the two coupled modes. The applications of differential antennas were highlighted, which clearly reveal that differential antennas play a very important role in the high-level integration of wireless systems. Finally, it must be stressed that the historic concept of lower gains and bulkier sizes of differential antennas compared single-ended counterpart antennas does not always hold true. For instance, differential microstrip patch antennas can offer comparable or even smaller sizes and higher gain values than single-ended microstrip patch antennas.

Acknowledgments

This author would like to thank Junjun Wang, Mei Sun, Bing Zhang, Zihao Chen, Zhihong Tu, Tianwei Deng, Zi-

jian Shao, Guanghui Xu, Jun Shu, Yaowei Hou, Yulin Fang, Zhihao Zhu, Wenmei Zhang, and Lin Zhang for their contribution in the research and development of differential antennas.

References

- [1] H. Hertz, *Electric Waves*, Macmillan, London, UK, 1893.
- [2] G. Marconi, "Transmitting electrical signals," *Patent*, 0586193, USA, 1897-06-13.
- [3] J. Ramsay, "Highlights of antenna history," *IEEE Communications Magazine*, vol. 19, no. 5, pp. 4–8, 1981.
- [4] H. Yagi, "Beam transmission of ultra short waves," *Proceedings of the Institute of Radio Engineers*, vol. 16, no. 6, pp. 715–740, 1928.
- [5] A. Blumlein, "Improvements in or relating to high frequency electrical conductors or radiators," *Patent*, 515684, UK, 1938-03-07.
- [6] J. D. Kraus, "The helical antenna," *Proceedings of the IRE*, vol. 37, no. 3, pp. 263–272, 1949.
- [7] J. D. Dyson, "The equiangular spiral antenna," *IRE Transactions on Antennas and Propagation*, vol. 7, no. 2, pp. 181–187, 1959.
- [8] R. DuHamel and D. Isbell, "Broadband logarithmically periodic antenna structures," in *Proceedings of 1958 IRE International Convention Record*, New York, NY, USA, pp. 119–128, 1957.
- [9] E. V. Byron, "A new flush-mounted antenna element for phased array application," in *Proc. 1970 Phased Array Antenna Symp.*, Polytechnic Institute of Brooklyn, New York, USA, pp. 187–192, 1970, Reprinted in *Phased Array Antennas*, ed. by A. A. Oliner and G. H. Knittel, Dedham: Artech House, 1972.
- [10] S. Long, M. McAllister, and L. Shen, "The resonant cylindrical dielectric cavity antenna," *IEEE Transactions on Antennas and Propagation*, vol. 31, no. 3, pp. 406–412, 1983.
- [11] J. D. Kraus, *Antennas*, 2nd Edition, McGraw-Hill, New Delhi, India, 1987.
- [12] Y. P. Zhang, J. J. Wang, Q. Li, *et al.*, "Antenna-in-package and transmit-receive switch for single-chip radio transceivers of differential architecture," *IEEE Transactions on Circuits and Systems I: Regular Papers*, vol. 55, no. 11, pp. 3564–3570, 2008.
- [13] P. R. Gray and R. G. Meyer, *Analysis and Design of Analog Integrated Circuits*, Wiley, New York, NY, USA, 1977.
- [14] Y. P. Zhang and J. J. Wang, "Theory and analysis of differentially-driven microstrip antenna," *IEEE Transactions on Antennas and Propagation*, vol. 54, no. 4, pp. 1092–1099, 2006.
- [15] Q. Xue, X. Y. Zhang, and C. H. K. Chin, "A novel differential-fed patch antenna," *IEEE Antennas and Wireless Propagation Letters*, vol. 5, pp. 471–474, 2006.
- [16] C. H. K. Chin, Q. Xue, and H. Wong, "Broadband patch antenna with a folded plate pair as a differential feeding scheme," *IEEE Transactions on Antennas and Propagation*, vol. 55, no. 9, pp. 2461–2467, 2007.
- [17] Y. P. Zhang, "Design and experiment on differentially-driven microstrip antennas," *IEEE Transactions on Antennas and Propagation*, vol. 55, no. 10, pp. 2701–2708, 2007.
- [18] L. P. Han, W. M. Zhang, X. W. Chen, *et al.*, "Design of compact differential dual-frequency antenna with stacked patches," *IEEE Transactions on Antennas and Propagation*, vol. 58, no. 4, pp. 1387–1392, 2010.
- [19] S. V. Hum and H. Y. Xiong, "Analysis and design of a differentially-fed frequency agile microstrip patch antenna," *IEEE Transactions on Antennas and Propagation*, vol. 58, no. 10, pp. 3122–3130, 2010.
- [20] Y. P. Zhang, "Electrical separation and fundamental resonance of differentially-driven microstrip antennas," *IEEE Transactions on Antennas and Propagation*, vol. 59, no. 4, pp. 1078–1084, 2011.
- [21] Y. C. Ou and G. M. Rebeiz, "Differential microstrip and slot-ring antennas for millimeter-wave silicon systems," *IEEE Transactions on Antennas and Propagation*, vol. 60, no. 6, pp. 2611–2619, 2012.
- [22] Y. P. Zhang, "Enrichment of package antenna approach with dual

- feeds, guard ring, and fences of vias," *IEEE Transactions on Advanced Packaging*, vol. 32, no. 3, pp. 612–618, 2009.
- [23] Z. J. Shao and Y. P. Zhang, "Miniaturization of differentially-driven microstrip planar inverted F antenna," *IEEE Transactions on Antennas and Propagation*, vol. 67, no. 2, pp. 1280–1283, 2019.
- [24] Z. J. Shao and Y. P. Zhang, "Differential shorted patch antennas," *IEEE Transactions on Antennas and Propagation*, vol. 67, no. 7, pp. 4438–4444, 2019.
- [25] T. Brauner, R. Vogt, and W. Bachtold, "A differential active patch antenna element for array applications," *IEEE Microwave and Wireless Components Letters*, vol. 13, no. 4, pp. 161–163, 2003.
- [26] W. Wang and Y. P. Zhang, "0.18- μm CMOS push-pull power amplifier with antenna in IC package," *IEEE Microwave and Wireless Components Letters*, vol. 14, no. 1, pp. 13–15, 2004.
- [27] U. R. Pfeiffer, J. Grzyb, D. X. Liu, *et al.*, "A chip-scale packaging technology for 60-GHz wireless chipsets," *IEEE Transactions on Microwave Theory and Techniques*, vol. 54, no. 8, pp. 3387–3397, 2006.
- [28] L. Zhang and Y. P. Zhang, "Differential grid array antenna to radiate pencil beam at 24 GHz," *IET Microwaves, Antennas & Propagation*, vol. 8, no. 10, pp. 765–769, 2014.
- [29] H. L. Peng, Z. Tang, Y. P. Zhang, *et al.*, "Cavity model analysis of a dual-probe-feed circular microstrip patch antenna," *IEEE Antennas and Wireless Propagation Letters*, vol. 15, pp. 44–47, 2015.
- [30] N. W. Liu, L. Zhu, W. W. Choi, *et al.*, "A novel differential-fed patch antenna on stepped-impedance resonator with enhanced bandwidth under dual-resonance," *IEEE Transactions on Antennas and Propagation*, vol. 64, no. 11, pp. 4618–4625, 2016.
- [31] G. H. Xu, H. L. Peng, C. L. Sun, *et al.*, "Differential probe fed liquid crystal-based frequency tunable circular ring patch antenna," *IEEE Access*, vol. 6, pp. 3051–3058, 2017.
- [32] J. P. Wang, Q. W. Liu, and L. Zhu, "Bandwidth enhancement of a differential-fed equilateral triangular patch antenna via loading of shorting posts," *IEEE Transactions on Antennas and Propagation*, vol. 65, no. 1, pp. 36–43, 2017.
- [33] N. W. Liu, L. Zhu, and W. W. Choi, "A differential-fed microstrip patch antenna with bandwidth enhancement under operation of TM_{10} and TM_{30} modes," *IEEE Transactions on Antennas and Propagation*, vol. 65, no. 4, pp. 1607–1614, 2017.
- [34] Y. W. Hou, Z. J. Shao, Y. P. Zhang, *et al.*, "A wideband differentially fed dual-polarized laminated resonator antenna," *IEEE Transactions on Antennas and Propagation*, vol. 69, no. 7, pp. 4148–4153, 2021.
- [35] Y. L. Fang and Y. P. Zhang, "On surface-wave suppression of differential circular microstrip antennas," *IEEE Antennas and Wireless Propagation Letters*, vol. 20, no. 9, pp. 1691–1695, 2021.
- [36] Y. X. Zhao, X. W. Zhu, and W. L. Song, "A 2×2 dual-polarized magneto-electric dipole antenna array at 28 GHz," in *Proceedings of 2021 IEEE International Symposium on Antennas and Propagation and USNC-URSI Radio Science Meeting*, Singapore, pp. 1–2, 2021.
- [37] Y. P. Zhang, "Impedance relations for differential antennas and single-ended counterparts," *IEEE Transactions on Antennas and Propagation*, vol. 70, no. 2, pp. 953–959, 2022.
- [38] Y. W. Hou, Y. P. Zhang, Z. J. Shao, *et al.*, "Theoretical and experimental investigations on differential aperture-coupled rectangular laminated resonator antenna," *IEEE Antennas and Wireless Propagation Letters*, vol. 21, no. 6, pp. 1213–1217, 2022.
- [39] Y. W. Hou, Y. P. Zhang, Z. J. Shao, *et al.*, "Theory and analysis on radiation characteristics of differential rectangular laminated resonator antenna," *IEEE Transactions on Antennas and Propagation*, vol. 70, no. 8, pp. 6365–6376, 2022.
- [40] Z. H. Tu and Y. P. Zhang, "Comparison of three methods for the measurement of the differential impedance of a balanced device," *IEEE Antennas and Propagation Magazine*, vol. 55, no. 5, pp. 142–151, 2013.
- [41] R. Meys and F. Janssens, "Measuring the impedance of balanced antennas by an S-parameter method," *IEEE Antennas and Propagation Magazine*, vol. 40, no. 6, pp. 62–65, 1998.
- [42] K. D. Palmer and M. W. van Rooyen, "Simple broadband measurements of balanced loads using a network analyzer," *IEEE Transactions on Instrumentation and Measurement*, vol. 55, no. 1, pp. 266–272, 2006.
- [43] Y. P. Zhang and Z. H. Tu, "Measuring the impedance and efficiency of differentially driven microstrip antenna by two balun methods," *IEEE Transactions on Antennas and Propagation*, vol. 62, no. 3, pp. 1246–1252, 2014.
- [44] C. R. Curry, "How to calibrate through balun transformers to accurately measure balanced systems," *IEEE Transactions on Microwave Theory and Techniques*, vol. 51, no. 3, pp. 961–965, 2003.
- [45] D. M. Pozar and B. Kaufman, "Comparison of three methods for the measurement of printed antenna efficiency," *IEEE Transactions on Antennas and Propagation*, vol. 36, no. 1, pp. 136–139, 1988.
- [46] H. Choo, R. Rogers, and H. Ling, "On the Wheeler cap measurement of the efficiency of microstrip antennas," *IEEE Transactions on Antennas and Propagation*, vol. 53, no. 7, pp. 2328–2332, 2005.
- [47] Y. P. Zhang and Z. H. Chen, "The Wheeler method for the measurement of the efficiency of differentially-driven microstrip antennas," *IEEE Transactions on Antennas and Propagation*, vol. 62, no. 6, pp. 3436–3439, 2014.
- [48] Y. L. Fang and Y. P. Zhang, "Theory and analysis of the loop antenna and Ω -shaped loop-dipole antenna," *IEEE Open Journal of Antennas and Propagation*, vol. 3, pp. 1161–1171, 2022.
- [49] J. E. Storer, "Impedance of thin-wire loop antennas," *Transactions of the American Institute of Electrical Engineers, Part I: Communication and Electronics*, vol. 75, no. 5, pp. 606–619, 1956.
- [50] B. Rao, "Far field of large circular loop antennas: Theoretical and experimental results," *IEEE Transactions on Antennas and Propagation*, vol. 16, no. 2, pp. 269–270, 1968.
- [51] S. S. Zhong, *Antenna Theory and Techniques*, Publishing House of Electronics Industry, Beijing, China, 2011. (in Chinese)
- [52] H. G. Booker, "Slot aeriels and their relation to complementary wire aeriels (Babinet's principle)," *Journal of the Institution of Electrical Engineers - Part IIIA: Radiolocation*, vol. 93, no. 4, pp. 620–626, 1946.
- [53] R. Munson, "Microstrip phased array antennas," in *Proceedings of 1973 EIC 11th Electrical Insulation Conference*, Chicago, IL, USA, pp. 281–283, 1973.
- [54] J. Q. Howell, "Microstrip antennas," in *Proceedings of 1972 Antennas and Propagation Society International Symposium*, Williamsburg, VA, USA, pp. 177–180, 1972.
- [55] R. E. Munson, "Conformal microstrip antennas and microstrip phased arrays," *IEEE Transactions on Antennas and Propagation*, vol. 22, no. 1, pp. 74–78, 1974.
- [56] J. Q. Howell, "Microstrip antennas," *IEEE Transactions on Antennas and Propagation*, vol. 23, no. 1, pp. 90–93, 1975.
- [57] K. R. Carver and J. W. Mink, "Microstrip antenna technology," *IEEE Transactions on Antennas and Propagation*, vol. 29, no. 1, pp. 2–24, 1981.
- [58] T. Chiba, Y. Suzuki, and N. Miyano, "Suppression of higher modes and cross polarized component for microstrip antennas," in *Proceedings of 1982 Antennas and Propagation Society International Symposium*, Albuquerque, NM, USA, pp. 285–288, 1982.
- [59] J. Hanfling, "Experimental results illustrating performance limitations and design tradeoffs in probe-fed microstrip-patch element phased arrays," in *Proceedings of 1986 Antennas and Propagation Society International Symposium*, Philadelphia, PA, USA, pp. 11–14, 1986.
- [60] J. J. Schuss and J. D. Hanfling, "Nonreciprocity and scan blindness in phased arrays using balanced-fed radiators," *IEEE Transactions on Antennas and Propagation*, vol. 35, no. 2, pp. 134–138, 1987.
- [61] R. L. Bauer and J. J. Schuss, "Axial ratio of balanced and unbalanced fed circularly polarized patch radiator arrays," in *Proceedings of 1987 Antennas and Propagation Society International Symposium*, Blacksburg, VA, USA, pp. 286–289, 1987.
- [62] J. J. Schuss, J. D. Hanfling, and R. E. Morrow, "Observation of scan

- blindness due to surface wave resonance in an array of printed circuit patch radiators," in *Proceedings of 1987 Antennas and Propagation Society International Symposium*, Blacksburg, VA, USA, pp. 802–805, 1987.
- [63] Z. Q. Tong, A. Stelzer, and W. Menzel, "Improved expressions for calculating the impedance of differential feed rectangular microstrip patch antennas," *IEEE Microwave and Wireless Components Letters*, vol. 22, no. 9, pp. 441–443, 2012.
- [64] P. S. Hall, C. Wood, and C. Garrett, "Wide bandwidth microstrip antennas for circuit integration," *Electronics Letters*, vol. 15, no. 15, pp. 458–460, 1979.
- [65] Z. J. Shao, L. F. Qiu, and Y. P. Zhang, "Design of wideband differentially fed multilayer stacked patch antennas based on bat algorithm," *IEEE Antennas and Wireless Propagation Letters*, vol. 19, no. 7, pp. 1172–1176, 2020.
- [66] C. W. Garvin, R. E. Munson, L. T. Ostwald, *et al.*, "Missile base mounted microstrip antennas," *IEEE Transactions on Antennas and Propagation*, vol. 25, no. 5, pp. 604–610, 1977.
- [67] T. Taga and K. Tsunekawa, "Performance analysis of a built-in planar inverted F antenna for 800 MHz band portable radio units," *IEEE Journal on Selected Areas in Communications*, vol. 5, no. 5, pp. 921–929, 1987.
- [68] J. D. Kraus, "A backward angle-fire array antenna," *IEEE Transactions on Antennas and Propagation*, vol. 12, no. 1, pp. 48–50, 1964.
- [69] R. Conti, I. Toth, T. Dowling, *et al.*, "The wire grid microstrip antenna," *IEEE Transactions on Antennas and Propagation*, vol. 29, no. 1, pp. 157–166, 1981.
- [70] Y. X. Qian, W. R. Deal, N. Kaneda, *et al.*, "Microstrip-fed quasi-Yagi antenna with broadband characteristics," *Electronics Letters*, vol. 34, no. 23, pp. 2194–2196, 1998.
- [71] Z. H. Zhu and Y. P. Zhang, "Design and analysis of differential quasi-Yagi antenna and array," *ZTE Communications*, under review, 2022.
- [72] C. Puente, J. Romeu, R. Pous, *et al.*, "Fractal multiband antenna based on the Sierpinski gasket," *Electronics Letters*, vol. 32, no. 1, pp. 1–2, 1996.
- [73] Y. L. Fang and Y. P. Zhang, "Printed fractal Sierpinski gasket dipole antenna with a novel planar feeding structure," in *Proceedings of 2022 IEEE Region 10 Conference*, Hong Kong, China, pp. 1–4, 2022.
- [74] V. H. Rumsey, "Frequency independent antennas," in *Proceedings of 1958 IRE International Convention Record*, New York, NY, USA, pp. 114–118, 1957.
- [75] M. McFadden and W. R. Scott, "Analysis of the equiangular spiral antenna on a dielectric substrate," *IEEE Transactions on Antennas and Propagation*, vol. 55, no. 11, pp. 3163–3171, 2007.
- [76] Y. Mushiaki, "The input impedance of a slit antenna," in *Proceedings of Joint Convention Record of Tohoku Sections of IEE and IECE of Japan*, pp. 25–26, June 1948.
- [77] K. W. Leung, K. M. Luk, K. Y. A. Lai, *et al.*, "Input impedance of hemispherical dielectric resonator antenna," *Electronics Letters*, vol. 27, no. 24, pp. 2259–2260, 1991.
- [78] B. Li and K. W. Leung, "On the differentially fed rectangular dielectric resonator antenna," *IEEE Transactions on Antennas and Propagation*, vol. 56, no. 2, pp. 353–359, 2008.
- [79] X. S. Fang, K. W. Leung, E. H. Lim, *et al.*, "Compact differential rectangular dielectric resonator antenna," *IEEE Antennas and Wireless Propagation Letters*, vol. 9, pp. 662–665, 2010.
- [80] C. X. Hao, B. Li, K. W. Leung, *et al.*, "Frequency-tunable differentially fed rectangular dielectric resonator antennas," *IEEE Antennas and Wireless Propagation Letters*, vol. 10, pp. 884–887, 2011.
- [81] S. J. Guo, L. S. Wu, K. W. Leung, *et al.*, "Microstrip-fed differential dielectric resonator antenna and array," *IEEE Antennas and Wireless Propagation Letters*, vol. 17, no. 9, pp. 1736–1739, 2018.
- [82] H. Tang, J. X. Chen, W. W. Yang, *et al.*, "Differential dual-band dual-polarized dielectric resonator antenna," *IEEE Transactions on Antennas and Propagation*, vol. 65, no. 2, pp. 855–860, 2017.
- [83] C. W. Tong, H. Tang, W. Qin, *et al.*, "Differentially inserted-fed compact dual-band circularly polarized dielectric resonator antenna," *IEEE Antennas and Wireless Propagation Letters*, vol. 18, no. 12, pp. 2498–2502, 2019.
- [84] H. Tang, C. W. Tong, and J. X. Chen, "Differential dual-polarized filtering dielectric resonator antenna," *IEEE Transactions on Antennas and Propagation*, vol. 66, no. 8, pp. 4298–4302, 2018.
- [85] H. Tang, X. W. Deng, and J. Shi, "Wideband substrate integrated differential dual-polarized dielectric resonator antenna," *IEEE Antennas and Wireless Propagation Letters*, vol. 21, no. 1, pp. 203–207, 2022.
- [86] H. L. Tian, Z. J. Chen, L. Chang, *et al.*, "Differentially fed duplex filtering dielectric resonator antenna with high isolation and CM suppression," *IEEE Transactions on Circuits and Systems II: Express Briefs*, vol. 69, no. 3, pp. 979–983, 2022.
- [87] C. Chen, J. X. Chen, and W. Hong, "Differentially fed dual-polarized 2-D multibeam dielectric resonator antenna array based on printed ridge gap waveguide," *IEEE Transactions on Antennas and Propagation*, vol. 70, no. 9, pp. 7967–7977, 2022.
- [88] "UWB circularly polarized ultra-wideband antenna spiral antenna isometric spiral antenna," Available at: <https://www.aliexpress.com/item/4000615104176.html>.
- [89] S. Miyazaki, "They said it couldn't be done, so we did it: Introducing the QTM052 mmWave antenna module family," Available at: <https://www.qualcomm.com/news/onq/2018/07/they-said-it-couldnt-be-done-so-we-did-it-introducing-qtm052-mmwave-antenna>, 2018-07-31.
- [90] X. X. Gu, D. X. Liu, Y. Hasegawa, *et al.*, "Antenna-in-package integration for a wideband scalable 5G millimeter-Wave phased-array module," *IEEE Microwave and Wireless Components Letters*, vol. 31, no. 6, pp. 682–684, 2021.
- [91] M. Sun, Y. P. Zhang, K. M. Chua, *et al.*, "Integration of Yagi antenna in LTCC package for differential 60-GHz radio," *IEEE Transactions on Antennas and Propagation*, vol. 56, no. 8, pp. 2780–2783, 2008.
- [92] I. Nasr, R. Jungmaier, A. Baheti, *et al.*, "A highly integrated 60 GHz 6-channel transceiver with antenna in package for smart sensing and short-range communications," *IEEE Journal of Solid-State Circuits*, vol. 51, no. 9, pp. 2066–2076, 2016.
- [93] F. Bauer, X. Wang, W. Menzel, *et al.*, "A 79-GHz radar sensor in LTCC technology using grid array antennas," *IEEE Transactions on Microwave Theory and Techniques*, vol. 61, no. 6, pp. 2514–2521, 2013.
- [94] A. Hamidipour, A. Fischer, M. Jahn, *et al.*, "160-GHz SiGe-based transmitter and receiver with highly directional antennas in package," in *Proceedings of 2013 European Microwave Integrated Circuit Conference*, Nuremberg, Germany, pp. 81–84, 2013.
- [95] S. Jameson, E. Halpern, and E. Socher, "20.4 A 300GHz wirelessly locked 2x3 array radiating 5.4dBm with 5.1% DC-to-RF efficiency in 65nm CMOS," in *Proceedings of 2016 IEEE International Solid-State Circuits Conference*, San Francisco, CA, USA, pp. 348–349, 2016.
- [96] E. Ojefors, U. R. Pfeiffer, A. Lissauskas, *et al.*, "A 0.65 THz focal-plane array in a quarter-micron CMOS process technology," *IEEE Journal of Solid-State Circuits*, vol. 44, no. 7, pp. 1968–1976, 2009.
- [97] Y. Y. Hu, S. Sun, H. Xu, *et al.*, "Grid-array rectenna with wide angle coverage for effectively harvesting RF energy of low power density," *IEEE Transactions on Microwave Theory and Techniques*, vol. 67, no. 1, pp. 402–413, 2019.
- [98] H. Wang, Y. Feng, and Y. X. Guo, "A differentially fed antenna with complex impedance for ingestible wireless capsules," *IEEE Antennas and Wireless Propagation Letters*, vol. 21, no. 1, pp. 139–143, 2022.
- [99] W. Lin and R. W. Ziolkowski, "Wireless power transfer (WPT) enabled IoT sensors based on ultra-thin electrically small antennas," in *Proceedings of the 2021 15th European Conference on Antennas and Propagation*, Düsseldorf, Germany, pp. 1–4, 2021.



Yueping Zhang is a Full Professor with the School of Electrical and Electronic Engineering at Nanyang Technological University, Singapore.

Prof. Zhang is a Fellow of the IEEE, was an Associate Editor of the *IEEE Transactions on Antennas and Propagation*, a Member of the IEEE Antennas and Propagation Society (IEEE APS) Field Award Committee, and a Distinguished Lecturer of the IEEE APS. He has published numerous papers, including two invited and one standard paper in the *Proceedings of the IEEE*, one invited paper in the *IEEE Transactions on Antennas and Propagation*, and one historical article in the *IEEE Antennas and Propagation Magazine*. He received the 2012 IEEE AP-S Sergei A. Schelkunoff Prize Paper Award.

Prof. Zhang has been invited to deliver plenary speeches at flagship conferences organized by both national and international societ-

ies. He received the Best Paper Award from the 2nd IEEE/IET International Symposium on Communication Systems, Networks and Digital Signal Processing, July 18–20, 2000, Bournemouth, U.K., the Best Paper Prize from the 3rd IEEE International Workshop on Antenna Technology, March 21–23, 2007, Cambridge, UK, and the Best Paper Award from the 10th IEEE Global Symposium on Millimeter-Waves, May 24–26, 2017, Hong Kong, China. He holds 7 US patents and has made pioneering and significant contributions to the development of antenna-in-package (AiP) technology. He received the 2020 IEEE AP-S John Kraus Antenna Award. He also received the 2022 Exceptional Technical Achievement Award from the IEEE Electronics Packaging Society. His current interests are in the development of antenna-on-chip (AoC) technology for very large-scale antenna integration and characterization of chip-scale propagation channels at terahertz for wireless chip area network (WCAN).

(Email: eypzhang@ntu.edu.sg)